

Article

The Mixed Variable Transfer Matrix Method and Its Application in Predicting the Frequency Domain Vibration Characteristics of Hydraulic Pipelines

Fuming Zhou ^{1,2}, Jian Liao ^{1,2,*}, Zongbin Chen ^{1,2}, Xiaopeng Tan ^{1,2} and Lin He ^{1,2}

¹ Institute of Noise & Vibration, Naval University of Engineering, Wuhan 430033, China; d22182402@nue.edu.cn (F.Z.)

² Nation Key Laboratory on Ship Vibration & Noise, Wuhan 430033, China

* Correspondence: jl_zss@163.com

Abstract: The fluid–structure interaction effect should not be disregarded when examining the vibration characteristics of hydraulic pipeline systems. The transfer matrix method (TMM) is an efficacious method for analyzing the vibration characteristics of hydraulic pipelines in the frequency domain, offering advantages such as simplicity and efficiency. However, the TMM suffers the problem of high frequency instability when dealing with long-span hydraulic pipelines, which restricts its practical application. Currently, several modified transfer matrix methods face challenges such as low computational efficiency and difficulties in handling complex boundaries. In response to these issues, this paper proposes a novel modified transfer matrix method known as the mixed variable transfer matrix method. This innovative method possesses clear physical significance and effectively prevents the transfer matrix from becoming singular without necessitating the subdivision of the pipeline length. Consequently, it addresses high-frequency instability while maintaining high computational efficiency. Moreover, this method is capable of addressing complex boundary problems by integrating boundary matrices, thereby demonstrating enhanced applicability compared to existing methods. The performance of the proposed method was validated through the utilization of classic Dube pipeline impact test data, and the result shows maximum errors of 3.03% relative to the public data. Subsequently, an experiment was conducted on a section of hydraulic piping within a ship’s steering system. A hydraulic fluid noise generator was established to induce fluid pulsation excitation to the pipeline, thereby simulating the actual boundary conditions encountered in a ship’s hydraulic pipeline system so as to corroborate the efficacy of the proposed method in predicting the frequency domain vibration characteristics of a real hydraulic pipeline system. The experimental results indicate that the proposed method offers significant advantages in terms of high precision, efficiency, and stability, shows maximum errors of 4.35% relative to experimental data, and demonstrates promising prospects for engineering applications.

Keywords: hydraulic pipeline; fluid–structure interaction; frequency domain vibration characteristics; mixed variable transfer matrix method



Citation: Zhou, F.; Liao, J.; Chen, Z.; Tan, X.; He, L. The Mixed Variable Transfer Matrix Method and Its Application in Predicting the Frequency Domain Vibration Characteristics of Hydraulic Pipelines. *Appl. Sci.* **2024**, *14*, 10847. <https://doi.org/10.3390/app142310847>

Academic Editor: Sergey Suslov

Received: 23 October 2024

Revised: 12 November 2024

Accepted: 20 November 2024

Published: 23 November 2024



Copyright: © 2024 by the authors. Licensee MDPI, Basel, Switzerland. This article is an open access article distributed under the terms and conditions of the Creative Commons Attribution (CC BY) license (<https://creativecommons.org/licenses/by/4.0/>).

1. Introduction

Hydraulic pipeline systems offer significant advantages, including high power density and exceptional stiffness under load. They are extensively utilized in the fields of aviation, aerospace, and the ship industry for the efficient transfer of power flow, energy flow, and mass flow [1–3]. In the ship industry, the design of hydraulic pipeline systems has historically prioritized function, often neglecting the critical aspects of vibration and noise. In reality, hydraulic pipeline systems have emerged as significant sources of vibrational radiation within ship environments. This is primarily due to factors such as pump-induced flow pulsations, environmental vibration, and fluid–structure interaction characteristics [4].

As underwater vessels, including submarine and unmanned underwater vehicles, increasingly demand high levels of acoustic stealth performance, it has become imperative to investigate the vibration and noise characteristics of hydraulic pipeline systems, as well as their control methods.

Fluid–structure interaction (FSI) is a critical aspect that must not be overlooked when examining the vibration of hydraulic pipeline systems. In the past decades, many scholars have studied pipeline FSI regarding many aspects, such as mechanism explanation [5,6], model construction [7] and engineering applications [8]. Pipeline FSI belongs to one of the general FSI. For hydraulic pipeline systems, the noise excitation source is usually the pulsating pressure of the fluid, so the nonlinear effect is usually ignored in the analysis process while the fluid–solid interaction between the pipeline and the fluid medium in the linear domain is emphasized. There are three types of interaction between fluid and the pipeline: Poisson coupling, friction coupling, and junction coupling. Poisson coupling and friction coupling exert their effects on the entire pipeline and can be described using first-order partial differential equations. In contrast, junction coupling primarily occurs at points of discontinuity in the pipeline or where there is a change in the direction of fluid flow; it must be expressed in conjunction with the pipeline equation and relevant boundary conditions. The pipeline FSI model has evolved from a classical water hammer model, which solely accounts for the characteristics of fluid pressure waves, to a comprehensive 14-equation model based on the Timoshenko beam theory. This advanced model incorporates not only the axial and lateral motions but also the torsional dynamics of the pipeline [9,10]. In terms of computational methods, it primarily encompasses the method of characteristics (MOC), the finite element method (FEM), and the transfer matrix method (TMM). The MOC is a widely utilized method for addressing hyperbolic partial differential equations. In the domain of pipeline FSI, it is frequently employed for the time-domain transient response analysis of pressure waves within the pipeline. Wiggert et al. [7] applied the MOC to investigate the pressure and stress responses in a spatially filled pipe featuring an elbow joint when the valve closes abruptly based on a 14-equation model. Tijsseling et al. [11] integrated an eight-equation model with the MOC to analyze the impact response of a planar liquid-filled elbow, providing an in-depth discussion on various boundary conditions. Xu and Jiao [12] introduced an MOC based on the modified compatibility equation, and this method improved algorithm accuracy by circumventing simplifications associated with this equation. Nevertheless, the MOC is subject to multiple interpolation errors related to characteristic lines and presents challenges in managing complex boundary conditions within pipeline systems, which constrains its broader engineering applications [13]. The FEM is a powerful tool for analyzing the modal and dynamic response of structures, with numerous applications in the field of pipeline FSI. Based on the finite element theory, Luczko and Czerwinski [14] employed spline functions as shape functions to develop a motion model for a three-dimensional liquid-filled pipeline. Based on the 14-equation beam model, Sreejith et al. [15] developed a finite element expression for pipelines that incorporated both Poisson coupling and junction coupling. The study focused on the water hammer effect as the target scenario. The findings indicate that neglecting FSI can lead to an overestimation of the calculated structural velocity. Furthermore, through recognizing the advantages of the MOC in addressing fluid dynamic characteristics alongside the efficacy of the FEM in handling structural vibration, many researchers have utilized the MOC-FEM to investigate pipeline FSI characteristics [16,17]. However, it is important to note that the FEM represents both pipe movement and fluid behavior through nodes and elements; thus, its accuracy and efficiency are contingent upon the number of discrete elements utilized. For complex long-span pipelines, the FEM incurs substantial computational costs, which remains a primary factor limiting its broader engineering application.

For ship hydraulic pipeline systems, frequency domain response characteristics are of paramount importance. The TMM serves as an effective tool for analyzing the frequency domain vibration characteristics of chain-linked systems. This method discretizes the system into a series of sets comprising domain transfer matrices and point transfer

matrices. By sequentially connecting these matrices, a global transfer matrix is formed, which incorporates boundary conditions to facilitate the realization of system modes and responses. This approach offers significant advantages in terms of both simplicity and efficiency. Tentarelli [10] examines the impact of frequency-domain-related friction terms, categorizing the state variables in the 14-equation model into a pair of conjugate groups. He derives the transfer matrix for pipes based on the general solution form of the wave equation. Liu and Li [18] transformed the axial, transverse, and torsional vibration models of straight pipes from multivariate first-order equations to one-dimensional high-order equations, thereby obtaining analytical solutions for each state variable and subsequently deriving the transfer matrix; however, this approach is limited to straight pipes. Zhang et al. [19] utilized the decoupling method of the MOC and introduced the L-MOC to derive the transfer matrix for the axial four equations governing straight pipe sections. This methodology has since become a classic technique for constructing transfer matrices in liquid-filled pipes. Building upon Zhang et al.'s work, Xu et al. [20] developed a solution addressing pipeline frequency-domain characteristics that incorporates complex constraints and extended the L-MOC method to encompass the 14-equation model.

In fact, although the methods for constructing transfer matrices in the aforementioned literature differ, they all address partial differential equations to derive the transfer relationships of state variables at both ends of the pipeline and are fundamentally interconnected. Several studies have indicated that numerical instability arises when calculating the frequency domain characteristics of long-span liquid-filled pipelines using the TMM based on the 14-equation model. Research conducted by De Jong [21] and Li [22] highlighted that this instability primarily occurs during calculations involving lateral vibrations of pipelines. Furthermore, investigations by Deng et al. [8] demonstrated that in systems containing curved pipes, axial excitation can also induce instability due to the coupling between axial and lateral vibrations within these curved structures.

In order to address the high-frequency instability issues associated with the TMM, various enhanced methods have been proposed sequentially. Tanaka et al. [23] introduced the concept of branching within the original system, which enhances TMM stability by integrating a side branch system into the boundary of the main path system, thereby shortening the transfer distance between variables. Wang [24] elaborated on this method's calculation process in detail based on Tanaka's theory; however, it necessitates constructing a complex intermediate matrix and is not universally applicable. The Riccati Transfer Matrix Method (RTMM) offers a means to reduce the dimensions of the transfer matrix while simultaneously improving stability by transforming a two-point boundary value problem into a one-point initial value problem. Nonetheless, this approach is limited to simple boundary conditions and proves unsuitable for intricate hydraulic pipelines [13,25]. Uhrig et al. [26] and Tentarelli et al. [5,6] proposed corresponding enhancement strategies for applying the TMM to tackle instability challenges in structural dynamics and the pipeline fluid–structure interaction (FSI). Although their computational processes differ, they all fundamentally segment the original system into distinct sub-elements to minimize the “characteristic length”. This treatment methodology is uniformly referred to as the Piecewise Transfer Matrix Method (PTMM) herein. De Jong and Li proposed a foundational framework for dividing subunits in the context of liquid-filled piping problems using the PTMM [21,27]. Subsequently, Deng et al. [8] applied the PTMM to analyze the frequency domain characteristics of aviation hydraulic piping systems. Similar to the FEM, the accuracy and stability of the PTMM are contingent upon the number of sub-elements. As pipeline system complexity increases, the dimensions of the global transfer matrix derived from the PTMM also expand, leading to decreased efficiency and thereby limiting its applicability. In addressing elastic wave propagation in layered media, Zhang et al. [28] introduced a method known as the mixed variable transfer matrix method. The central premise involves transforming the traditional transfer matrix into a mixed variable transfer matrix. Here, “mixed variable” refers to utilizing potential variables at one end of the system alongside flow variables at the opposite end as fundamental parameters. Cao et al. [29] were pioneers in applying this method within

pipeline FSI contexts and demonstrated its effectiveness; however, their investigations were confined to simple straight pipes under ideal boundary conditions, leaving further exploration regarding this method's broader applicability unaddressed.

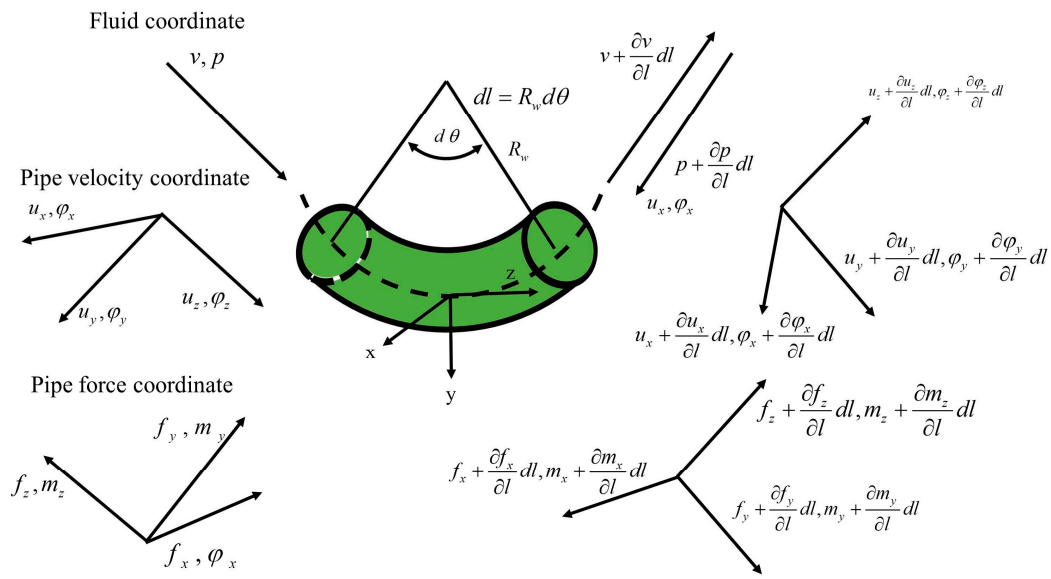
Ship hydraulic pipelines typically span long distances in space. Given this context, it is essential to develop an efficient, accurate, and stable method for analyzing the FSI frequency domain characteristics of long-span hydraulic pipelines. This paper constructs the frequency-domain transfer matrix for a typical hydraulic pipeline based on the FSI 14-equation model and employs the concept of mixed variable matrices. Furthermore, we derived a recursive algorithm for the mixed variable transfer matrix, enabling the effective prediction of the frequency domain vibration response of the hydraulic pipeline by incorporating the matrix representation of complex boundary constraints. This approach is also referred to as the mixed variable transfer matrix method (MVTMM) in this paper. The proposed method was validated using FSI test data published by Dube University and through an FSI module developed within commercial finite element software. Subsequently, we conducted experiments on a section of a U-shaped pipeline utilized in a ship's steering device. It is important to note that previous experiments concerning FSI in pipelines predominantly involved free boundary conditions based on force hammer impact methods [30,31], which differ significantly from the operational environment encountered in actual hydraulic pipeline systems. In relation to steering gear applications, fluid pulsations at the pipe's terminus represent a primary source of radiated noise. Therefore, this study simulates realistic boundary conditions pertinent to ship hydraulic pipeline systems and completes an experimental investigation into the frequency domain vibration response of the target pipeline under fluid excitation combined with a fluid noise generator. This work substantiates the engineering applicability of our proposed method.

The structure of this paper is organized as follows: In the Section 2, an FSI 14-equation model for a hydraulic pipeline, incorporating Friction coupling, is established. Additionally, the theory of the classical TMM is summarized and its instability mechanisms are analyzed. After that, the fundamental principles of the MVTMM, including the recursive algorithm and matrix representation for complex boundaries, culminating in a comprehensive frequency-domain characteristic analysis method tailored for FSI in pipelines is described in detail. Section 3 validates the performance of the proposed method using data from the Dube pipeline and the FEM. In Section 4, an experimental investigation into the FSI vibration characteristics of a U-shaped hydraulic pipeline under fluid excitation is conducted to demonstrate the engineering applicability of this method. Section 5 concludes with final remarks.

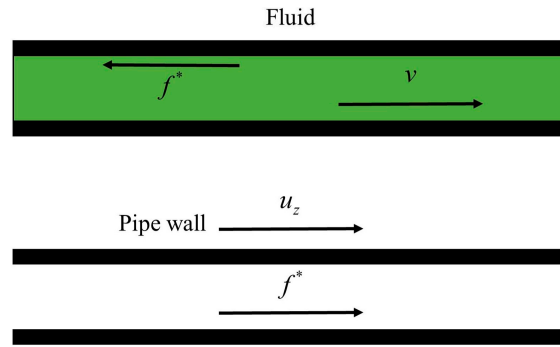
2. Overview of the TMM

2.1. The 14-Equation Model for FSI in Hydraulic Pipelines

The 14-equation model, based on the Timoshenko beam, comprehensively characterizes the dynamic relationship between potential variables (force, moment) and flow variables (velocity, angular velocity) across each degree of freedom in the hydraulic pipeline. This model currently represents the most complete framework for describing the FSI characteristics inherent to pipelines. It comprises four equations that address axial vibrations of the pipeline, eight equations pertaining to transverse vibrations, and two equations related to torsional vibrations. Figure 1 illustrates both the force analysis diagram of a microelement within the elbow section and a schematic representation of axial friction coupling between the pipe and fluid. By considering the force conditions acting on the microelement of both the pipe and fluid, a 14-equation model that incorporates friction coupling can be established, while the detailed derivation process of the model can be found in reference [10], which is not described in detail in this paper due to space reasons.



(a) Analysis of forces acting on microelement of curved pipeline.



(b) The schematic diagram of friction coupling

Figure 1. A schematic representation of force for a liquid-filled pipeline microelement.

The equations of axial motion are as follows:

$$\frac{\partial p}{\partial l} = -\rho_f \frac{\partial v}{\partial t} - \frac{2\tau}{r_i \rho_f} \tag{1}$$

$$\frac{\partial v}{\partial l} = \left(-\frac{1}{K} - \frac{(1 - \mu^2)(2r_i + e)}{Ee}\right) \frac{\partial p}{\partial t} + \frac{2\mu}{EA_p} \frac{\partial f_z}{\partial t} - \frac{u_y}{R_w} \tag{2}$$

$$\frac{\partial f_z}{\partial l} = A_p \rho_p \frac{\partial u_z}{\partial t} - 2\pi r_i \tau - \frac{f_y}{R_w} \tag{3}$$

$$\frac{\partial u_z}{\partial z} = \frac{1}{EA_p} \frac{\partial f_z}{\partial t} - \frac{\mu r_i}{Ee} \frac{\partial p}{\partial t} - \frac{u_y}{R} \tag{4}$$

The equations of lateral motion in the y-z plane are as follows:

$$\frac{\partial f_y}{\partial l} = (\rho_f A_f + \rho_p A_p) \frac{\partial u_y}{\partial t} + \frac{f_z}{R_w} - \frac{A_f}{R_w} p \tag{5}$$

$$\frac{\partial u_y}{\partial l} = \frac{1}{k^2 G A_p} \frac{\partial f_y}{\partial t} - \varphi_x + \frac{u_z}{R_w} \tag{6}$$

$$\frac{\partial m_x}{\partial l} = (\rho_p I_p + \rho_f I_f) \frac{\partial \varphi_x}{\partial t} + f_y \tag{7}$$

$$\frac{\partial \varphi_x}{\partial l} = E_A \frac{\partial m_x}{\partial t} \tag{8}$$

The equations of lateral motion in the x-z plane are as follows:

$$\frac{\partial f_x}{\partial l} = (\rho_f A_f + \rho_p A_p) \frac{\partial u_x}{\partial t} \tag{9}$$

$$\frac{\partial u_x}{\partial l} = \frac{1}{k^2 G A_p} \frac{\partial f_x}{\partial t} + \varphi_y \tag{10}$$

$$\frac{\partial m_y}{\partial l} = (\rho_p I_p + \rho_f I_f) \frac{\partial \varphi_y}{\partial t} - f_x + \frac{m_z}{R_w} \tag{11}$$

$$\frac{\partial \varphi_y}{\partial l} = E_A \frac{\partial m_y}{\partial t} + \frac{\varphi_z}{R_w} \tag{12}$$

The equations of motion about the z axis are as follows:

$$\frac{\partial m_z}{\partial l} = \rho_p J_p \frac{\partial \varphi_z}{\partial t} - \frac{m_y}{R_w} \tag{13}$$

$$\frac{\partial \varphi_z}{\partial l} = \frac{1}{G J_p} \frac{\partial m_z}{\partial t} - \frac{1}{R_w} \varphi_y \tag{14}$$

where $k^2 = 2 \frac{1+\mu}{4+3\mu}$ is identified as the shear constant. E_A denotes the bending rigidity of the pipe. $E_A = \frac{1}{E I_p}$ applies when the object is a straight pipe, while $E_A = \frac{ff}{E I_p}$ pertains to cases involving a curved pipe. ff represents the rigidity correction factor, which is stated in Equation (15). It is worth noting that the meaning of all the variables involved in the theoretical derivation of this paper can be found in the nomenclature.

$$ff = \frac{1.65 r_i^2}{e R_w} \tag{15}$$

It can be observed from Equations (1) to (14) that both friction coupling and Poisson coupling are present in the axial four equations. In the transverse plane, the fluid exerts an additional mass effect on the pipe. For straight pipes, axial and transverse vibrations are decoupled; however, for curved pipes, these vibrations are coupled with one another. Consequently, the vibration characteristics of curved pipes exhibit greater complexity.

2.2. The Classic TMM and the Analysis of Its Instability Mechanism

The derivation of the classical TMM has been completed by previous researchers, and the details can be seen in Appendix A [19,20]. This is not the main innovation of this paper, so it will not be elaborated here. It can be observed from the derivation presented in Appendix A that the field transfer matrix of the pipeline includes an exponential term, denoted as $\exp(-sl/\lambda)$, whose value is significantly influenced by both the length and frequency of the pipeline. When the frequency remains constant, an increase in the pipeline length leads to exponential changes in the values of corresponding elements within the transfer matrix; some elements may experience a sharp increase while others approach zero. This phenomenon results in an escalation of the condition number of the transfer matrix towards singularity, which can cause instability during matrix inversion operations on a computer. Similarly, when maintaining a constant length, variations in frequency also induce exponential changes in element values within the transfer matrix. The same instability arises with increasing analysis frequencies. Thus, fundamentally speaking, stability issues associated with the transfer matrix represent a mathematical challenge. Li et al. [25] have mathematically demonstrated that for FSI involving pipelines, the condition number of the axial transfer matrix is consistently equal to 1; conversely, it has been established that there exists a positive correlation between both the length and frequency

and the condition number of transverse transfer matrices. Consequently, for a simple straight pipeline, instabilities related to this method primarily manifest during solutions concerning transverse vibration.

2.3. The Theory of the MVTMM

To enhance the high-frequency stability of the TMM, numerous studies have embraced a segmented approach. This involves subdividing the pipeline system into several shorter sub-segments based on specific criteria, followed by increasing the matrix dimensions through node coupling, which is called the PTMM. This strategy aims to improve algorithmic stability, albeit at the cost of computational efficiency. The introduction of the PTMM can be found in Appendix B. As indicated in Equation (A13), the dimension of the node-coupling matrix increases with the number of tube segments. Specifically, this matrix is a square matrix with a dimension of $14 \times (N + 1)$, whereas the transfer matrix consistently maintains a dimension of 14×14 . Consequently, the efficiency of the PTMM is inferior to that of the TMM. For long-span hydraulic piping systems, it is imperative to develop a new method that balances both efficiency and accuracy.

2.3.1. The Construction of the Mixed Variable Transfer Matrix

The 14 frequency-domain state variables of the hydraulic pipeline system are organized into pairs of conjugate variable groups based on symmetry, specifically $\mathbf{Var} = \{P, F_z, U_y, M_x, F_x, \psi_y, M_z\}$ and $\mathbf{Var}_c = \{V, U_z, F_y, \psi_x, U_x, M_y, \psi_z\}$. The concept of symmetry is discussed in the literature [10]. Subsequently, Equations (1)–(14) can be uniformly expressed in the following matrix form after applying Laplace transformation:

$$\frac{\partial}{\partial l} \begin{bmatrix} P \\ F_z \\ U_y \\ M_x \\ F_x \\ \psi_y \\ M_z \\ V \\ U_z \\ F_y \\ \psi_x \\ U_x \\ M_y \\ \psi_z \end{bmatrix} = \begin{bmatrix} 0 & 0 & 0 & 0 & 0 & 0 & 0 & D_1 & D_2 & 0 & 0 & 0 & 0 & 0 \\ 0 & 0 & 0 & 0 & 0 & 0 & 0 & D_3 & D_4 & \frac{-1}{R_w} & 0 & 0 & 0 & 0 \\ 0 & 0 & 0 & 0 & 0 & 0 & 0 & 0 & \frac{1}{R_w} & \frac{-1}{k^2 G A_p} & -1 & 0 & 0 & 0 \\ 0 & 0 & 0 & 0 & 0 & 0 & 0 & 0 & 0 & 1 & D_5 & 0 & 0 & 0 \\ 0 & 0 & 0 & 0 & 0 & 0 & 0 & 0 & 0 & 0 & 0 & D_6 & 0 & 0 \\ 0 & 0 & 0 & 0 & 0 & 0 & 0 & 0 & 0 & 0 & 0 & 0 & s E_A & \frac{1}{R_w} \\ 0 & 0 & 0 & 0 & 0 & 0 & 0 & 0 & 0 & 0 & 0 & 0 & \frac{-1}{R_w} & s \rho_p J_p \\ \frac{-s}{K^*} & \frac{2\mu s}{E A_p} & \frac{-1}{R_w} & 0 & 0 & 0 & 0 & 0 & 0 & 0 & 0 & 0 & 0 & 0 \\ D_7 & \frac{s}{E A_p} & \frac{-1}{R_w} & 0 & 0 & 0 & 0 & 0 & 0 & 0 & 0 & 0 & 0 & 0 \\ \frac{-A_f}{R_w} & \frac{1}{R_w} & D_6 & 0 & 0 & 0 & 0 & 0 & 0 & 0 & 0 & 0 & 0 & 0 \\ 0 & 0 & 0 & s E_A & 0 & 0 & 0 & 0 & 0 & 0 & 0 & 0 & 0 & 0 \\ 0 & 0 & 0 & 0 & \frac{s}{k^2 G A_p} & 1 & 0 & 0 & 0 & 0 & 0 & 0 & 0 & 0 \\ 0 & 0 & 0 & 0 & -1 & D_5 & \frac{1}{R_w} & 0 & 0 & 0 & 0 & 0 & 0 & 0 \\ 0 & 0 & 0 & 0 & 0 & \frac{-1}{R_w} & \frac{s}{G J_p} & 0 & 0 & 0 & 0 & 0 & 0 & 0 \end{bmatrix} \begin{bmatrix} P \\ F_z \\ U_y \\ M_x \\ F_x \\ \psi_y \\ M_z \\ V \\ U_z \\ F_y \\ \psi_x \\ U_x \\ M_y \\ \psi_z \end{bmatrix} \quad (16)$$

where

$$D_1 = -(\rho_f s + \frac{2\rho_f s}{\vartheta_1(jr_i \sqrt{s/v_f}) - 2}), \quad D_2 = \frac{2\rho_f s}{\vartheta_1(jr_i \sqrt{s/v_f}) - 2}, \quad D_3 = -\frac{2\pi\rho_f r_i^2 s}{\vartheta_1(jr_i \sqrt{s/v_f}) - 2},$$

$$D_4 = A_p \rho_p s + \frac{2\pi\rho_f r_i^2 s}{\vartheta_1(jr_i \sqrt{s/v_f}) - 2}, \quad D_5 = s\rho_p I_p + s\rho_f I_f, \quad \text{and } D_6 = s\rho_f A_f + s\rho_p A_p, \quad D_7 = -\frac{s\mu r_i}{Ee}.$$

Equation (16) can be abbreviated as follows:

$$\frac{\partial}{\partial l} \bar{\Phi}(l, s) = \mathbf{T}^*(s) \bar{\Phi}(l, s) \quad (17)$$

where $\bar{\Phi}(l, s) = \begin{bmatrix} \mathbf{Var}(l, s) \\ \mathbf{Var}_c(l, s) \end{bmatrix}, \mathbf{T}^*(s) = \begin{bmatrix} 0 & \mathbf{T}_{12}(s) \\ \mathbf{T}_{21}(s) & 0 \end{bmatrix}.$

$$(\mathbf{J}\mathbf{T}^*(s))^H = \mathbf{J}\mathbf{T}^*(s), \mathbf{J} = \begin{bmatrix} 0 & \mathbf{I} \\ -\mathbf{I} & 0 \end{bmatrix} \quad (18)$$

\mathbf{T} is a 14×14 square matrix that encapsulates all parameter information of the FSI 14-equation model. Furthermore, \mathbf{T} satisfies Equation (18), which implies that \mathbf{T} is a Hamiltonian matrix. According to the properties of Hamiltonian matrices, half of its eigenvalues correspond to the mechanical wave propagation constants traveling forward along the pipeline element, while the other half represent those propagating backward along the same element. Consequently, \mathbf{T} can be expressed as follows:

$$\mathbf{\Lambda}(s) = \mathbf{S}(s)^{-1} \mathbf{T}(s) \mathbf{S}(s) \tag{19}$$

where $\mathbf{\Lambda}(s) = \begin{bmatrix} \lambda(s)^U & 0 \\ 0 & \lambda(s)^D \end{bmatrix}$ is a square matrix with eigenvalues, $\mathbf{S}(s) = \begin{bmatrix} \mathbf{S}(s)^{UU} & \mathbf{S}(s)^{UD} \\ \mathbf{S}(s)^{DU} & \mathbf{S}(s)^{DD} \end{bmatrix}$ is a square matrix composed of the corresponding eigenvectors, and the superscripts U and D denote forward and reverse directions along the pipeline, respectively.

The process described is analogous to the decoupling procedure outlined in Equation (A4) and is derived through the transformation of Equation (17):

$$\frac{\partial}{\partial l} \boldsymbol{\eta}(l, s) = \mathbf{S}(s)^{-1} \mathbf{T}(s) \mathbf{S}(s) \boldsymbol{\eta}(l, s) = \mathbf{\Lambda}(s) \boldsymbol{\eta}(l, s) \tag{20}$$

The solution to Equation (20) can be articulated as follows:

$$\boldsymbol{\eta}(l, s) = \begin{bmatrix} \exp(\lambda^U(l - l_0)) & 0 \\ 0 & \exp(\lambda^D(l - l_1)) \end{bmatrix} \begin{bmatrix} A^{*,U} \\ A^{*,D} \end{bmatrix} \tag{21}$$

where l_0 and l_L denote the initial and final positions of the pipeline system, respectively, while $A^{*,U}$ and $A^{*,D}$ represent the amplitudes of the incident and reflected mechanical waves within the pipeline. Therefore, the following is true:

$$\begin{bmatrix} \mathbf{Var}(l, s) \\ \mathbf{Var}_c(l, s) \end{bmatrix} = \begin{bmatrix} \mathbf{S}(s)^{UU} & \mathbf{S}(s)^{UD} \\ \mathbf{S}(s)^{DU} & \mathbf{S}(s)^{DD} \end{bmatrix} \begin{bmatrix} \exp(\lambda^U(l - l_0)) & 0 \\ 0 & \exp(\lambda^D(l - l_1)) \end{bmatrix} \begin{bmatrix} A^{*,U} \\ A^{*,D} \end{bmatrix} \tag{22}$$

Let $\mathbf{\Lambda}(s)^U = \exp(\lambda(s)^U L)$ and $\mathbf{\Lambda}(s)^D = \exp(-\lambda(s)^D L)$, where $L = l_1 - l_0$ represents the length of the pipeline. This is in conjunction with the boundary conditions established at both ends of the pipeline:

$$\begin{bmatrix} \mathbf{Var}(l_0, s) \\ \mathbf{Var}_c(l_0, s) \end{bmatrix} = \begin{bmatrix} \mathbf{S}(s)^{UU} & \mathbf{S}(s)^{UD} \\ \mathbf{S}(s)^{DU} & \mathbf{S}(s)^{DD} \end{bmatrix} \begin{bmatrix} \mathbf{I} & 0 \\ 0 & \mathbf{\Lambda}(s)^D \end{bmatrix} \begin{bmatrix} A^{*,U} \\ A^{*,D} \end{bmatrix} = \begin{bmatrix} \mathbf{S}(s)^{UU} & \mathbf{S}(s)^{UD} \mathbf{\Lambda}(s)^D \\ \mathbf{S}(s)^{DU} & \mathbf{S}(s)^{DD} \mathbf{\Lambda}(s)^D \end{bmatrix} \begin{bmatrix} A^{*,U} \\ A^{*,D} \end{bmatrix} \tag{23}$$

$$\begin{bmatrix} \mathbf{Var}(l_1, s) \\ \mathbf{Var}_c(l_1, s) \end{bmatrix} = \begin{bmatrix} \mathbf{S}(s)^{UU} & \mathbf{S}(s)^{UD} \\ \mathbf{S}(s)^{DU} & \mathbf{S}(s)^{DD} \end{bmatrix} \begin{bmatrix} \mathbf{\Lambda}(s)^U & 0 \\ 0 & \mathbf{I} \end{bmatrix} \begin{bmatrix} A^{*,U} \\ A^{*,D} \end{bmatrix} = \begin{bmatrix} \mathbf{S}(s)^{UU} \mathbf{\Lambda}(s)^U & \mathbf{S}(s)^{UD} \\ \mathbf{S}(s)^{DU} \mathbf{\Lambda}(s)^U & \mathbf{S}(s)^{DD} \end{bmatrix} \begin{bmatrix} A^{*,U} \\ A^{*,D} \end{bmatrix} \tag{24}$$

Based on Equations (23) and (24), we can conclude the following:

$$\begin{bmatrix} \mathbf{Var}(l_1, s) \\ \mathbf{Var}_c(l_0, s) \end{bmatrix} = \begin{bmatrix} \mathbf{X}_{l_1, l_0} & -\mathbf{Z}_{l_1, l_0} \\ \mathbf{Y}_{l_1, l_0} & \mathbf{W}_{l_1, l_0} \end{bmatrix} \begin{bmatrix} \mathbf{Var}(l_0, s) \\ \mathbf{Var}_c(l_1, s) \end{bmatrix} \tag{25}$$

$$\begin{bmatrix} \mathbf{X}_{l_1, l_0} & -\mathbf{Z}_{l_1, l_0} \\ \mathbf{Y}_{l_1, l_0} & \mathbf{W}_{l_1, l_0} \end{bmatrix} = \begin{bmatrix} \mathbf{S}^{UU}(s) \mathbf{\Lambda}(s)^U & \mathbf{S}(s)^{UD} \\ \mathbf{S}(s)^{DU} & \mathbf{S}(s)^{DD} \mathbf{\Lambda}(s)^D \end{bmatrix} \begin{bmatrix} \mathbf{S}(s)^{UU} & \mathbf{S}(s)^{UD} \mathbf{\Lambda}(s)^D \\ \mathbf{S}(s)^{DU} \mathbf{\Lambda}(s)^U & \mathbf{S}(s)^{DD} \end{bmatrix}^{-1} \tag{26}$$

\mathbf{Z}_{l_1, l_0} and \mathbf{Y}_{l_1, l_0} can be interpreted as the impedance matrix and the admittance matrix of the pipeline, respectively. As indicated in Equation (25), the state vectors on both sides of the equation consist of variables at both ends of the pipeline; thus, they are referred to as mixed variable vectors. The corresponding transfer matrix is termed the mixed variable transfer matrix. From Equation (26), it is evident that the diagonal elements of the inverse matrix on its right side do not include exponential terms. Consequently, when the length of the

pipeline is substantial, this matrix remains non-singular. Conversely, for shorter pipelines, this matrix corresponds to an eigenvector matrix derived from the Hamiltonian matrix, which retains invertibility due to inherent properties associated with Hamiltonian matrices. Furthermore, by applying the recursive algorithm pertaining to mixed variable transfer matrices, we can derive a global transfer matrix for chain systems without necessitating additional operations involving inverse matrices. Therefore, employing mixed variable transfer matrices instead of traditional transfer matrices effectively mitigates high-frequency instability issues commonly encountered in long pipelines.

2.3.2. FSI Frequency Domain Solution of Hydraulic Pipeline Based on MVTMM

a. Boundary conditions

The boundary conditions play a crucial role in determining the characteristics of a pipeline. Figure 2 illustrates the schematic representation of the boundaries and constraints within the hydraulic pipeline system. In such systems, fluid boundary conditions are typically induced by pulsating pressure at one end, while they are constrained by a throttle valve at the opposite end. The pipeline’s boundary condition must be established based on the actual installation state of the pipeline, which can be modeled as a spring-damping system with six degrees of freedom. This paper focuses on the hydraulic pipeline associated with ship steering gear, where boundary conditions at both ends of the pipeline can be considered as fixed constraints.

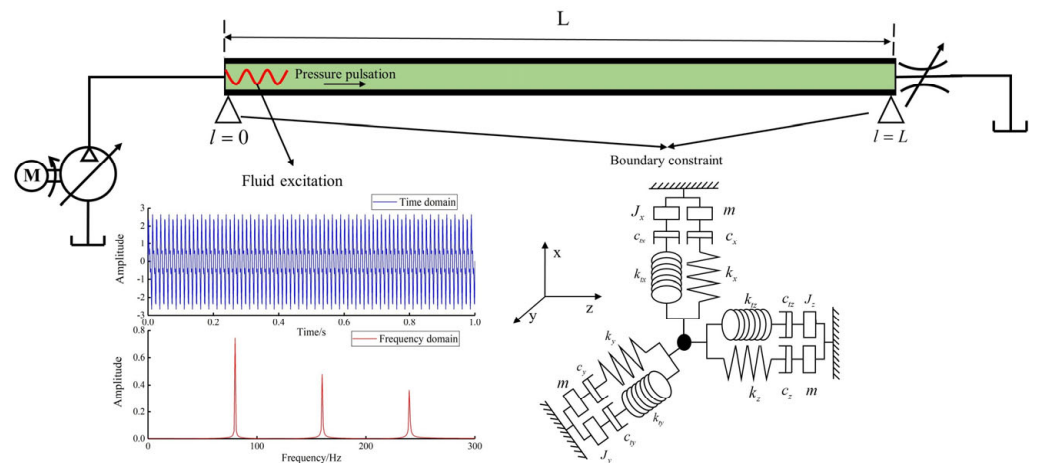


Figure 2. A schematic diagram of hydraulic pipeline boundaries and constraints.

The boundary conditions and excitations can be expressed in the form of a boundary matrix and an excitation vector. For the system illustrated in Figure 2:

The boundary conditions and excitation vector at $l = 0$ are as follows:

$$\mathbf{D}_s(s) = \begin{bmatrix} 1 & 0 & 0 & 0 & 0 & 0 & 0 & 0 & 0 & 0 & 0 & 0 & 0 & 0 \\ 0 & 1 & 0 & 0 & 0 & 0 & 0 & 0 & -Z_{zs} & 0 & 0 & 0 & 0 & 0 \\ 0 & 0 & -Z_{ys} & 0 & 0 & 0 & 0 & 0 & 0 & 1 & 0 & 0 & 0 & 0 \\ 0 & 0 & 0 & 1 & 0 & 0 & 0 & 0 & 0 & 0 & -Y_{xs} & 0 & 0 & 0 \\ 0 & 0 & 0 & 0 & 1 & 0 & 0 & 0 & 0 & 0 & 0 & -Z_{xs} & 0 & 0 \\ 0 & 0 & 0 & 0 & 0 & -Y_{ys} & 0 & 0 & 0 & 0 & 0 & 0 & 1 & 0 \\ 0 & 0 & 0 & 0 & 0 & 0 & 1 & 0 & 0 & 0 & 0 & 0 & 0 & -Y_{zs} \end{bmatrix}_{7 \times 14} \quad (27)$$

$$\mathbf{Q}_s(s) = [P \ 0 \ 0 \ 0 \ 0 \ 0 \ 0 \ 0] \quad (28)$$

The boundary conditions and excitation vector at $l = L$ are as follows:

$$\mathbf{D}_e(s) = \begin{bmatrix} 1 & 0 & 0 & 0 & 0 & 0 & 0 & -Z_v & 0 & 0 & 0 & 0 & 0 & 0 \\ 0 & 1 & 0 & 0 & 0 & 0 & 0 & 0 & Z_{ze} & 0 & 0 & 0 & 0 & 0 \\ 0 & 0 & Z_{ye} & 0 & 0 & 0 & 0 & 0 & 0 & 1 & 0 & 0 & 0 & 0 \\ 0 & 0 & 0 & 1 & 0 & 0 & 0 & 0 & 0 & 0 & Y_{xe} & 0 & 0 & 0 \\ 0 & 0 & 0 & 0 & 1 & 0 & 0 & 0 & 0 & 0 & 0 & Z_{xe} & 0 & 0 \\ 0 & 0 & 0 & 0 & 0 & Y_y & 0 & 0 & 0 & 0 & 0 & 0 & 1 & 0 \\ 0 & 0 & 0 & 0 & 0 & 0 & 1 & 0 & 0 & 0 & 0 & 0 & 0 & Y_{ze} \end{bmatrix}_{7 \times 14} \quad (29)$$

$$Q_e(s) = [0 \ 0 \ 0 \ 0 \ 0 \ 0 \ 0 \ 0] \quad (30)$$

$$Z_i = \frac{k_i}{s} + c_i + ms \quad (31)$$

$$Y_i = \frac{k_{ti}}{s} + c_{ti} + J_i s \quad (32)$$

In Equations (31) and (32), Z_i and Y_i denote the velocity impedance coefficients and angular velocity impedance coefficients, respectively, $i = x, y, z$. Additionally, k, c, k_t, c_t, m, J represent linear stiffness, linear damping, rotational stiffness, rotational damping, mass, and the moment of inertia. For the boundary conditions of fixed constraint, it is sufficient to assign maximum values to k and k_t , with a value of 1×10^{12} utilized in this study. Here, P signifies the Laplace transform of the fluid excitation signal and Z_v represents the fluid impedance associated with the throttle valve, which can be expressed as follows:

$$Z_v = 2A_f \frac{\Delta P}{Q} \quad (33)$$

where ΔP represents the pressure differential across the throttle valve, and Q denotes the flow rate within the piping system.

b. The recursive algorithm of MVTMM

For the chain system illustrated in Figure A1, it is necessary to derive a recursive algorithm to obtain the global transfer matrix. The mixed variable transfer matrix for the pipeline segment i can be expressed as follows:

$$\begin{bmatrix} \mathbf{Var}(l_i, s) \\ \mathbf{Var}_c(l_{i-1}, s) \end{bmatrix} = \begin{bmatrix} \mathbf{X}_{i,i-1} & -\mathbf{Z}_{i,i-1} \\ \mathbf{Y}_{i,i-1} & \mathbf{W}_{i,i-1} \end{bmatrix} \begin{bmatrix} \mathbf{Var}(l_{i-1}, s) \\ \mathbf{Var}_c(l_i, s) \end{bmatrix} \quad (34)$$

The mixed variable transfer matrix for the pipeline segment $i + 1$ can be expressed as follows:

$$\begin{bmatrix} \mathbf{Var}(l_{i+1}, s) \\ \mathbf{Var}_c(l_i, s) \end{bmatrix} = \begin{bmatrix} \mathbf{X}_{i+1,i} & -\mathbf{Z}_{i+1,i} \\ \mathbf{Y}_{i+1,i} & \mathbf{W}_{i+1,i} \end{bmatrix} \begin{bmatrix} \mathbf{Var}(l_i, s) \\ \mathbf{Var}_c(l_{i+1}, s) \end{bmatrix} \quad (35)$$

Combining Equations (34) and (35) yields the following:

$$\begin{bmatrix} \mathbf{Var}(l_{i+1}, s) \\ \mathbf{Var}_c(l_{i-1}, s) \end{bmatrix} = \begin{bmatrix} \mathbf{X}_{i+1,i-1} & -\mathbf{Z}_{i+1,i-1} \\ \mathbf{Y}_{i+1,i-1} & \mathbf{W}_{i+1,i-1} \end{bmatrix} \begin{bmatrix} \mathbf{Var}(l_{i-1}, s) \\ \mathbf{Var}_c(l_{i+1}, s) \end{bmatrix} \quad (36)$$

where

$$\begin{aligned}
 \mathbf{X}_{i+1,i-1} &= \mathbf{X}_{i+1,i}(\mathbf{I} + \mathbf{Z}_{i,i-1}\mathbf{Y}_{i+1,i})^{-1}\mathbf{X}_{i,i-1} \\
 \mathbf{Z}_{i+1,i-1} &= \mathbf{Z}_{i+1,i} + \mathbf{X}_{i+1,i}(\mathbf{Z}_{i,i-1}^{-1} + \mathbf{Y}_{i+1,i})^{-1}\mathbf{X}_{i+1,i}^H \\
 \mathbf{Y}_{i+1,i-1} &= \mathbf{Y}_{i,i-1} + \mathbf{X}_{i,i-1}^H(\mathbf{Y}_{i+1,i}^{-1} + \mathbf{Z}_{i,i-1})^{-1}\mathbf{X}_{i,i-1} \\
 \mathbf{W}_{i+1,i-1} &= \mathbf{W}_{i,i-1}(\mathbf{I} + \mathbf{Y}_{i+1,i}\mathbf{Z}_{i,i-1})^{-1}\mathbf{W}_{i+1,i}
 \end{aligned} \tag{37}$$

Therefore, the global transfer matrix for a hydraulic pipeline comprising N pipe segments is as follows:

$$\begin{bmatrix} \mathbf{Var}(l_{N,s}) \\ \mathbf{Var}_c(l_{0,s}) \end{bmatrix} = \mathbf{MVT}^{global} \begin{bmatrix} \mathbf{Var}(l_{0,s}) \\ \mathbf{Var}_c(l_{N,s}) \end{bmatrix} = \begin{bmatrix} \mathbf{X}_{N,0} & -\mathbf{Z}_{N,0} \\ \mathbf{Y}_{N,0} & \mathbf{W}_{N,0} \end{bmatrix} \begin{bmatrix} \mathbf{Var}(l_{0,s}) \\ \mathbf{Var}_c(l_{N,s}) \end{bmatrix} \tag{38}$$

$$\begin{aligned}
 \mathbf{X}_{N,0} &= \mathbf{X}^N(\mathbf{I} + \mathbf{Z}_{N-1,0}\mathbf{Y}^N)^{-1}\mathbf{X}_{N-1,0} \\
 \mathbf{Z}_{N,0} &= \mathbf{Z}^N + \mathbf{X}^N(\mathbf{Z}_{N-1,0}^{-1} + \mathbf{Y}^N)^{-1}\mathbf{W}^N \\
 \mathbf{Y}_{N,0} &= \mathbf{Y}_{N-1,0} + \mathbf{W}_{N-1,0}((\mathbf{Y}^N)^{-1} + \mathbf{Z}_{N-1,0})^{-1}\mathbf{X}_{N-1,0} \\
 \mathbf{W}_{N,0} &= \mathbf{W}_{N-1,0}(\mathbf{I} + \mathbf{Y}^N\mathbf{Z}_{N-1,0})^{-1}\mathbf{W}^N
 \end{aligned} \tag{39}$$

In Equation (39), \mathbf{X}^n denotes the transfer matrix of the n -th pipe segment, and $\mathbf{X}_{N-1,0}$ signifies the global transfer matrix of the preceding $N - 1$ pipe segments. Consequently, the global transfer matrix for the entire pipeline system can be derived by iteratively applying Equations (34)–(37). Furthermore, Equations (27)–(30) are modified in accordance with the principles governing conjugate variables, as illustrated in Equation (40). Equation (41) can then be resolved through integration with Equation (39). Notably, the dimension of the global coefficient matrix in (41) remains constant at 28×28 , irrespective of the number of pipe segments involved. This characteristic contributes to a higher computational efficiency for the MVTMM compared to the PTMM.

$$\begin{aligned}
 \mathbf{D}_s^V(s)\mathbf{Var}(l_{0,s}) + \mathbf{D}_s^{Vc}(s)\mathbf{Var}_c(l_{0,s}) &= \mathbf{Q}_s(s) \\
 \mathbf{D}_e^V(s)\mathbf{Var}(l_{N,s}) + \mathbf{D}_e^{Vc}(s)\mathbf{Var}_c(l_{N,s}) &= \mathbf{Q}_e(s)
 \end{aligned} \tag{40}$$

$$\begin{bmatrix} 0 & \mathbf{D}_s^{Vc} & \mathbf{D}_s^V & 0 \\ \mathbf{I}_{7 \times 7} & 0 & \mathbf{X}_{N,0} & -\mathbf{Z}_{N,0} \\ 0 & \mathbf{I}_{7 \times 7} & \mathbf{Y}_{N,0} & \mathbf{W}_{N,0} \\ \mathbf{D}_e^V & 0 & 0 & \mathbf{D}_e^{Vc} \end{bmatrix}_{28 \times 28} \begin{bmatrix} \mathbf{Var}(l_{N,s}) \\ \mathbf{Var}_c(l_{0,s}) \\ \mathbf{Var}(l_{0,s}) \\ \mathbf{Var}_c(l_{N,s}) \end{bmatrix}_{28 \times 1} = \begin{bmatrix} \mathbf{Q}_s(s) \\ 0 \\ 0 \\ \mathbf{Q}_e(s) \end{bmatrix}_{28 \times 1} \tag{41}$$

Based on the above theoretical derivation, the process of the MVTMM-based research method for FSI frequency-domain vibration characteristics of hydraulic pipelines proposed in this paper can be intuitively expressed using Figure 3:

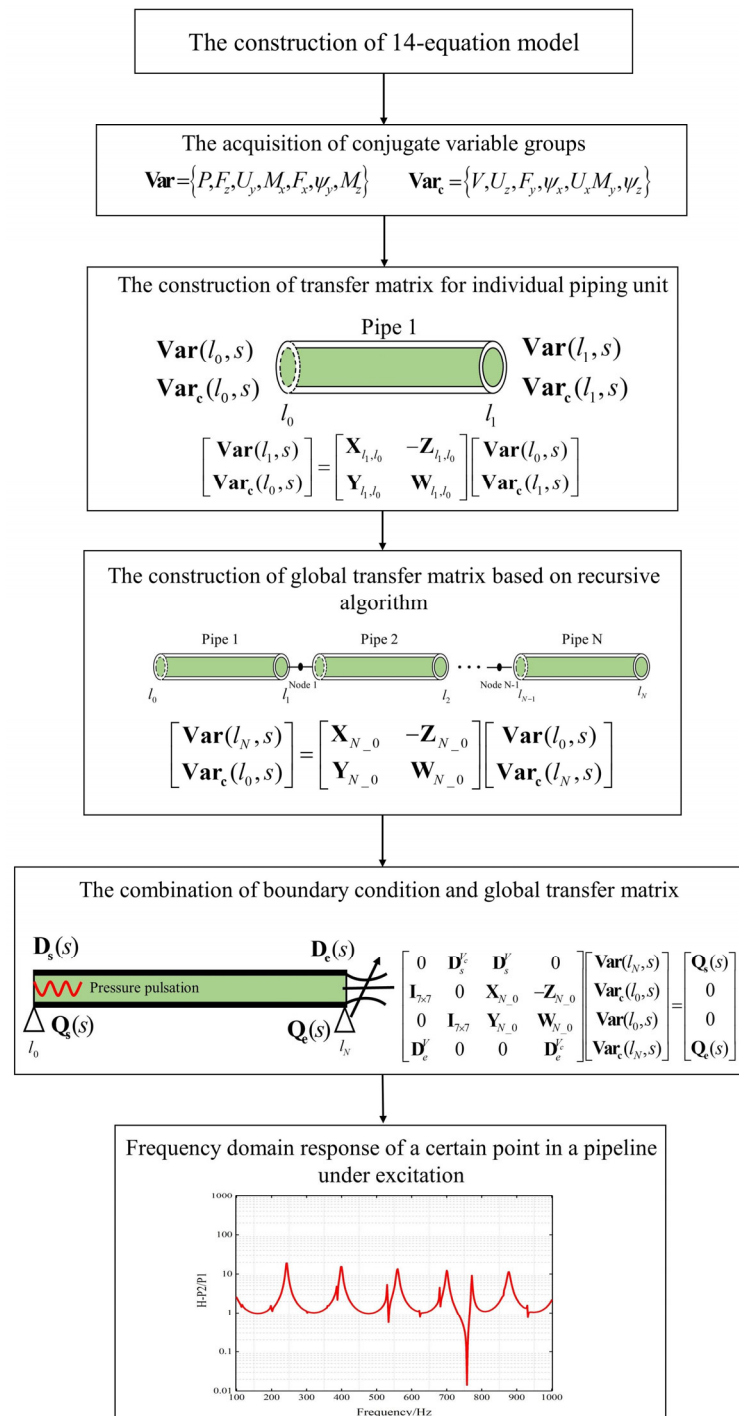


Figure 3. A flow chart of the proposed method.

3. Model Verification

Dubee University has conducted numerous classic FSI experiments on liquid-filled pipelines, encompassing both straight and elbow pipelines [32]. The resulting data have provided effective support for researchers to validate the accuracy of their models. In this section, we focus on a straight pipeline and an L-shaped elbow pipeline as examples to assess the performance of the proposed method. Both types of pipes are free-hanging, water-filled structures with closed ends. One end of the straight pipeline is subjected to a transverse exciting force, while one end of the elbow pipeline experiences an axial exciting force, as illustrated in Figure 4. The parameters for both the pipeline and fluid are detailed

in Table 1. The selection of these two cases was motivated by their representativeness and their ability to directly demonstrate the instability phenomena present in the TMM. To comprehensively evaluate the theoretical method’s performance, we employed an FSI module integrated into commercial finite element software to predict the frequency domain response of liquid-filled pipelines for cross-verification purposes. The parameter settings of the simulation model are the same as those described in the literature [8]. As depicted in Figure 5, the TMM effectively predicts the frequency domain response of pipelines within low-frequency ranges, aligning closely with the prediction results of the FEM. However, when assessing the transverse velocity response of the straight pipeline at frequencies exceeding 800 Hz, significant instability is observed. Similarly, instability arises in the frequency domain response of the L-elbow pipeline above 500 Hz. This indicates that the TMM possesses inherent limitations when addressing long-span pipelines; the explanations regarding these deficiencies can be found in Section 2.2.

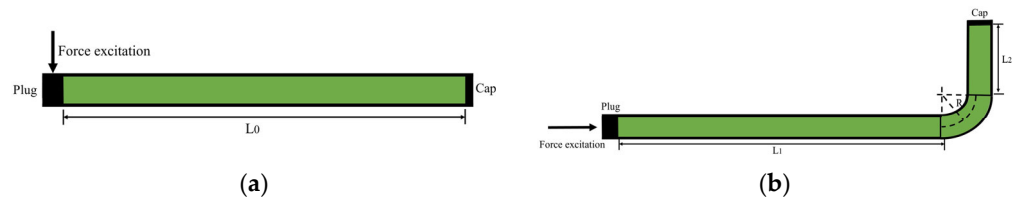


Figure 4. The liquid-filled pipelines used in the Dubee University experiment. (a) Straight pip–line, (b) L–elbow pipeline.

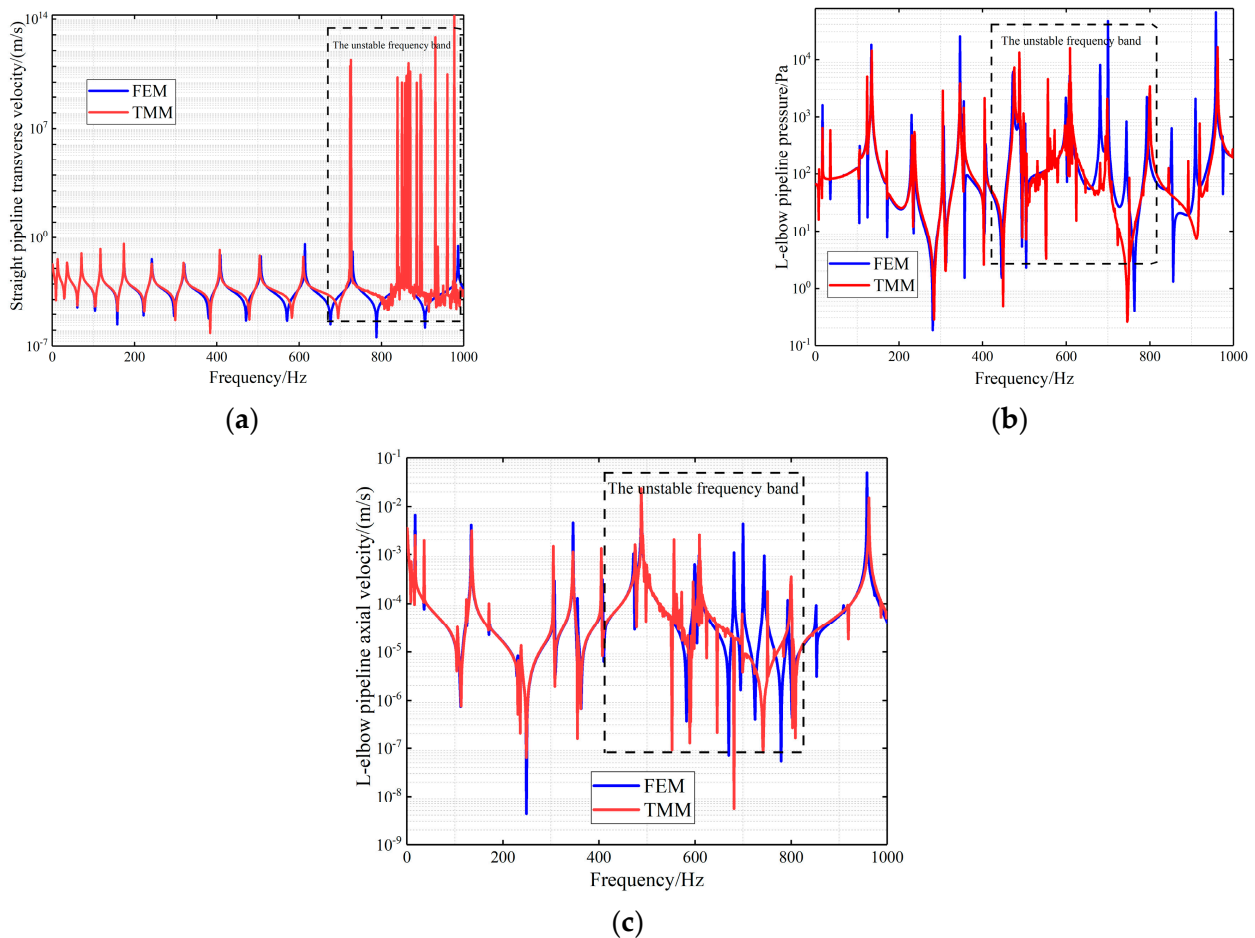


Figure 5. Frequency domain response of Dubee pipelines. (a) Transverse velocity response of straight pipeline, (b) Pressure response of L–elbow pipeline, (c) Axial velocity response of L–elbow pipeline.

Table 1. The parameters of the pipeline and fluid.

Pipeline		
Density: 7985kg/m ³	L0: 4.502 m	Inner radius: 0.02601 m
Young’s modulus: 168 GPa	L1: 4.435 m	Wall thickness: 0.003945 m
Poisson’s ratio: 0.29	Rw: 0.1013 m	
Shear coefficient: 0.53	L2: 1.263 m	
Fluid		
Density: 999 kg/m ³	Bulk modulus: 2.14 GPa	

The instability observed is associated with both the length of the pipeline and the frequency band utilized for solving. To address this instability issue, the MVTMM is employed to predict the frequency domain response of Dubee pipelines. The results are presented in Figure 6. It is evident that the processing outcomes from the MVTMM and the FME are largely consistent, effectively mitigating the instability problem.

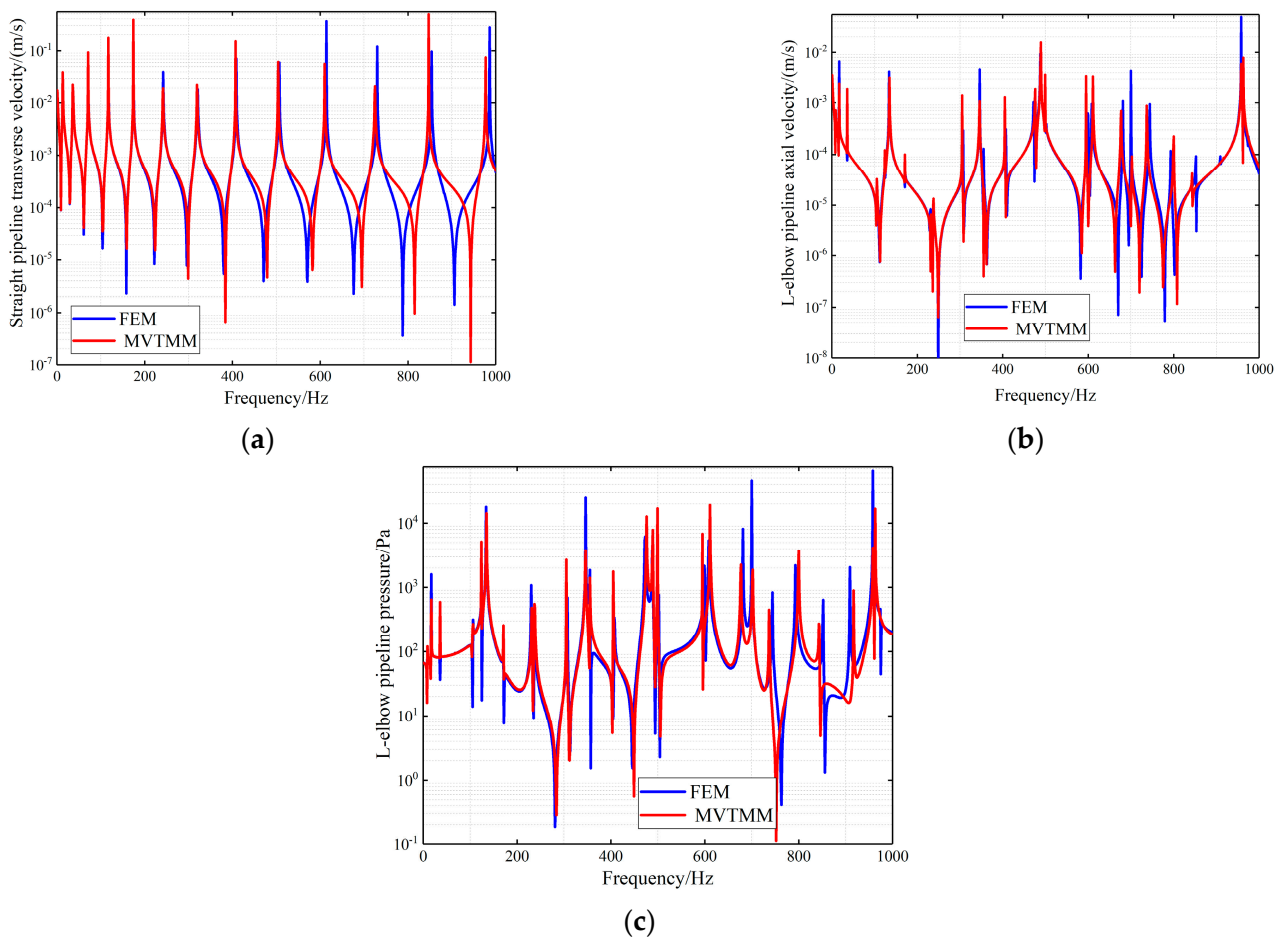


Figure 6. Frequency domain response of Dubee pipelines. (a) Transverse velocity response of straight pipeline, (b) Pressure response of L-elbow pipeline, (c) Axial velocity response of L-elbow pipeline.

Tables 2 and 3 provide a comparison between the natural frequencies calculated using the MVTMM, the TMM, the FEM, and those obtained from experiments. It can be seen that the results calculated by the FEM are basically consistent with the experiment, which proves the correctness of the simulation model. Then, it can be observed that the maximum error between the MVTMM and the experimental model is 3.03%, which substantiates that not only does our method resolve the instability issue, but it also demonstrates high predictive accuracy. In addition, it is worth noting that the calculation results in the stable

frequency band of the TMM are completely consistent with those of the MVTMM, which indicates that the main advantage of the MVTMM over the TMM is its ability to overcome its instability.

Table 2. Natural frequency of straight pipes: comparison between calculation and experiment.

The Experimental Result (Hz)	MVTMM		TMM		FEM	
	Natural Frequency (Hz)	Relative Error to Experiment (%)	Natural Frequency (Hz)	Relative Error to Experiment (%)	Natural Frequency (Hz)	Relative Error to Experiment (%)
13	13	0	13	0	13	0
36	36	0	36	0	36	0
70	71	1.43	71	1.43	71	1.43
116	117	0.86	117	0.86	117	0.86
173	174	0.58	174	0.58	174	0.58
241	242	0.41	242	0.41	242	0.41
320	319	0.31	319	0.31	321	0.31
411	407	0.97	407	0.97	409	0.48
510	504	1.18	504	1.18	507	0.59
619	610	1.45	610	1.45	614	0.81
737	725	1.63	-	-	730	0.95
864	847	1.97	-	-	854	1.16
999	977	2.2	-	-	986	1.3

Table 3. Natural frequency of L-elbow pipes: comparison between calculation and experiment.

The Experimental Result (Hz)	MVTMM		TMM		FEM	
	Natural Frequency (Hz)	Relative Error to Experiment (%)	Natural Frequency (Hz)	Relative Error to Experiment (%)	Natural Frequency (Hz)	Relative Error to Experiment (%)
9	9	0	9	0	9	0
17	17	0	17	0	17	0
35	36	2.86	36	2.86	37	5.71
66	68	3.03	68	3.03	68	3.03
104	105	0.96	105	0.96	106	1.92
124	124	0	124	0	124	0
136	135	0.74	135	0.74	134	1.47
168	171	1.79	171	1.79	172	2.38
231	231	0	231	0	231	0.00
239	238	0.42	238	0.42	238	0.42
303	305	0.66	305	0.66	307	1.32
346	346	0	346	0	346	0
361	356	1.39	356	1.39	355	1.66
401	405	1	405	1	407	1.50
473	476	0.63	476	0.63	472	0.21
483	489	1.24	489	1.24	488	1.04
499	499	0	499	0	502	0.60

4. Experimental Research

The Introduction of the Testing Equipment

In order to further validate the engineering application value of the proposed method, this section focuses on a DN25 U-elbow pipeline utilized in ship steering gears as the subject of experimental research. The configuration of the pipeline is illustrated in Figure 7. The material of the pipe is 304 stainless steel, and the fluid employed is No. 46 anti-wear hydraulic oil. The relevant parameters for both the pipeline and fluid are presented in Table 4. To obtain flue and structure vibration data, two high-precision pressure pulsation sensors, designated P1 and P2, were installed at both ends of the U-elbow pipeline to measure fluid noise within it. Additionally, an acceleration sensor labeled A1 was positioned at the midpoint of L2 to assess the transverse vibration of the pipeline. A significant challenge associated with FSI experiments lies in accurately establishing boundary conditions. To achieve a wide-band response from the U-elbow pipeline under fluid pulsation excitation, a dedicated fluid noise generator was developed for this study; its schematic representation can be found in Figure 8. The operational principle of this device is as follows: The motor-pump unit serves as a flow source that provides necessary flow and pressure for the system; concurrently, a vibration exciter drives a low-friction hydraulic cylinder acting as a

fluid noise source to generate pressure pulsation throughout the pipeline. Furthermore, a throttle valve located within an end rigid mass block supplies impedance loading for the pipeline. The primary advantage offered by this fluid noise generator lies in its ability to precisely adjust sinusoidal excitation frequencies via an upper computer to attain the desired frequencies of fluid pulsation while minimizing motor pump group-generated noise through the implementation of both pulsation attenuators and a long flexible hose. This configuration effectively decouples both the noise source and the flow source, thereby ensuring the acquisition of high signal-to-noise ratio (SNR) fluid noise across the entire frequency spectrum.

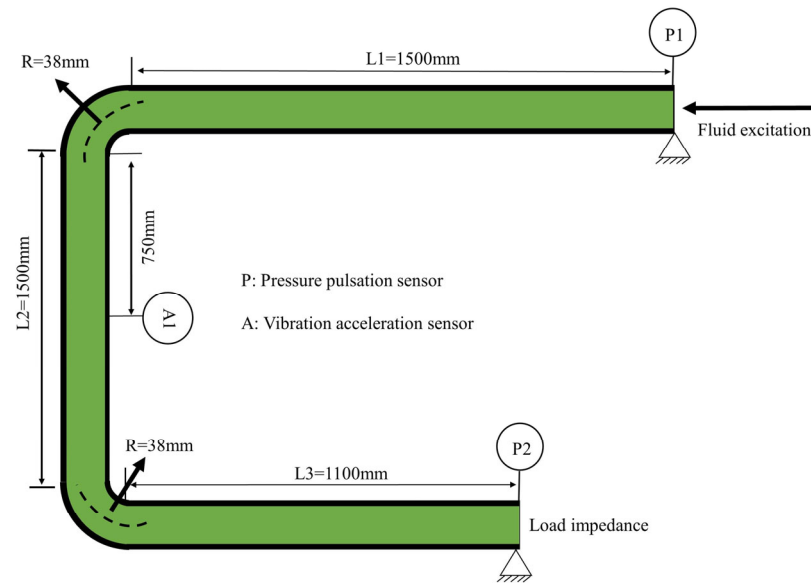


Figure 7. The configuration of the measured pipeline.

Table 4. The parameters of the pipeline and fluid.

Pipeline (Stainless Steel)		
Density: 7985 kg/m ³	L1: 1.5 m	R: 0.038 m
Young’s modulus: 206 GPa	L2: 1.5 m	Inner radius: 0.0125 m
Poisson’s ratio: 0.29	L3: 1.1 m	Wall thickness: 0.0045 m
Fluid (Hydraulic oil)		
Density: 876 kg/m ³	Bulk modulus: 1.68 GPa	Kinematic viscosity: 46 mm ² /s

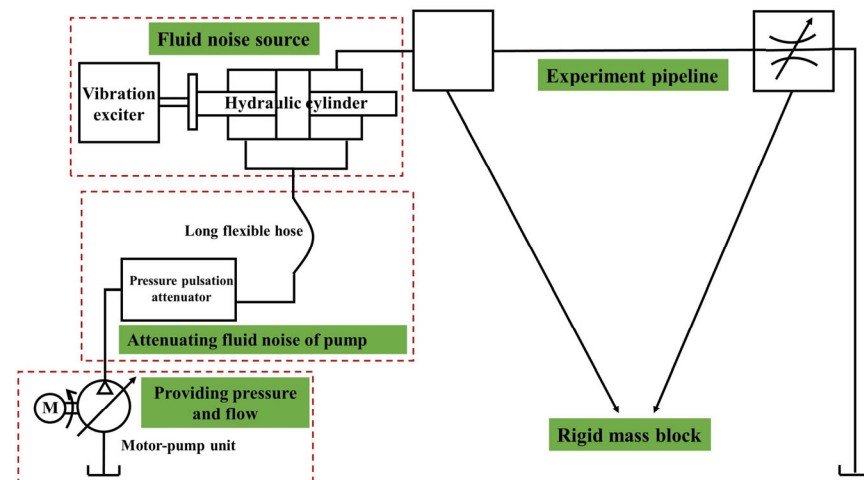


Figure 8. A schematic diagram of the fluid noise generator.

The experiment platform, illustrated in Figure 9, primarily comprised three components: the flow source and noise source, the data acquisition equipment, and the measured pipeline. Both ends of the pipeline were connected to a rigid mass block with sufficient weight, which can be considered as providing fixed constraints. During the experiment, the throttle valve was closed off while the system pressure was regulated via the relief valve located at the pump outlet. At this juncture, the impedance at the fluid's end approached infinity, effectively simulating a rigid boundary condition. Prior to the initiating test, the system operated under constant conditions for half an hour to mitigate any interference caused by bubbles within the pipeline. Throughout the experiment procedures, the temperature was maintained at 24 °C, with a flow rate of 36 L/min and a pressure of 10 MPa. The fluid noise generator delivered wide-band fluid excitation ranging from 100 Hz to 1 kHz for the measured pipeline; sweeping occurred in increments of 5 Hz with each single-frequency line spectrum held for a duration of 1.5 s. The time-frequency waterfall diagram recorded at point P1 is presented in Figure 10. It reveals that amplitude fluctuations in pressure occur periodically across various frequencies—this phenomenon correlates with specific distribution parameter characteristics inherent to the pipeline structure. Overall, it can be concluded that the fluid noise generator produces relatively high SNR fluid noise within the frequency band of 100 Hz to 1 kHz, thus serving as an effective excitation source for evaluating pipeline systems.

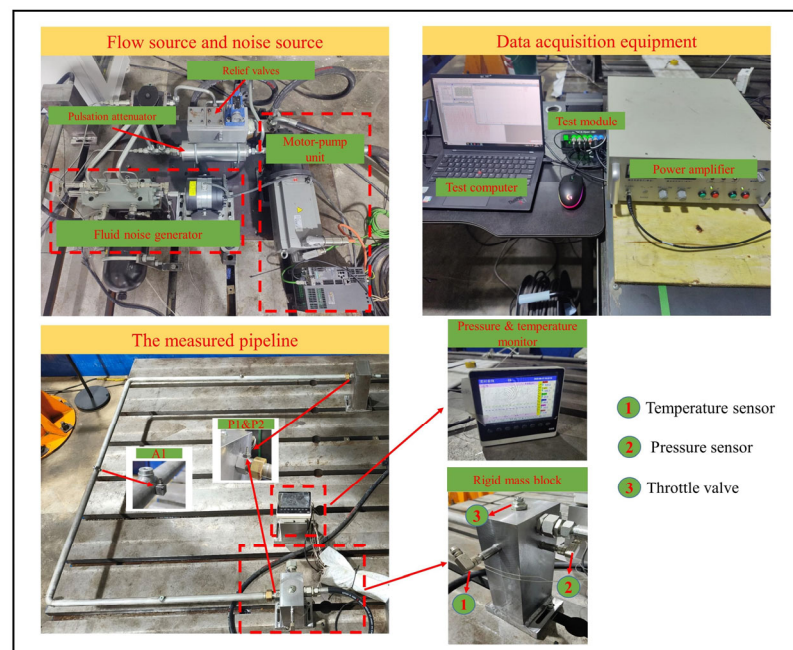


Figure 9. The experiment platform.

In order to evaluate the advantages of this method regarding computational stability, the two transfer functions defined in Table 5 were utilized as verification indicators. The pipeline was modeled using commercial finite element software. Both ends of the pipeline were subjected to fixed constraints, with the fluid end configured as a closed port. The input excitation applied was a unit of sound pressure. A comparison of the calculation results from the classical TMM, the MVTMM proposed in this paper, and the FEM is presented in Figure 11. As illustrated in Figure 11a, for the indicator H-P2/P1, the TMM exhibits instability within a frequency range above 600 Hz, rendering it incapable of accurately predicting the vibration characteristics of fluid dynamics in that frequency domain. In contrast, the MVTMM maintains stability across all frequencies and aligns closely with the FEM results. This observation underscores the MVTMM's advantage in enhancing result stability. Furthermore, it should be noted that the resonance peak values calculated via the FEM tend to be generally higher than those obtained through the TMM and the

MVTMM due to neglecting viscous friction effects within fluid modeling. Figure 11b further demonstrates that the TMM remains unstable at frequencies exceeding 500 Hz, making accurate predictions regarding pipeline flow-induced vibrations infeasible. Conversely, the MVTMM continues to exhibit stability throughout all frequency bands; its predicted natural frequencies align closely with those derived from the FEM analysis. A comparative assessment between theoretical predictions and simulation outcomes clearly indicates that the MVTMM possesses significant advantages over the TMM concerning stability.

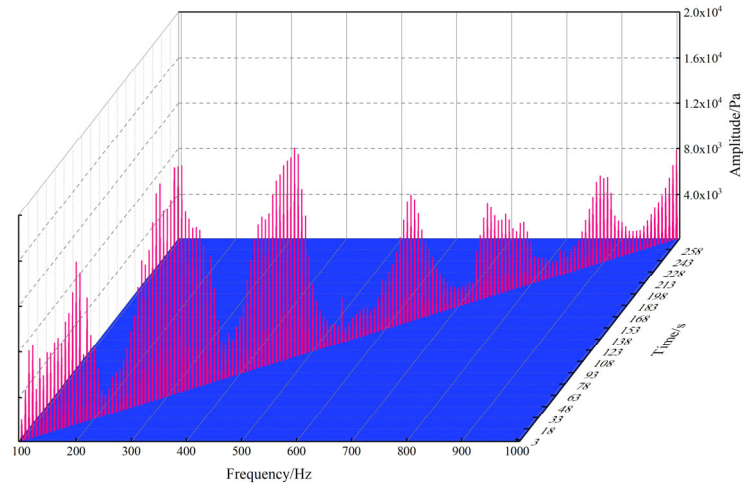


Figure 10. A time–frequency diagram of the pressure pulsation at point P1.

Table 5. The verification indicators.

Transfer Function	Mathematical Definition	Physical Significance
H-P2/P1	Pipeline outlet pulsating pressure/inlet pulsating pressure	Vibration characteristics of fluid inside pipeline
H-A1/P1	Pipeline vibration acceleration/pipeline inlet pulsating pressure	Fluid-induced vibration characteristics of pipeline

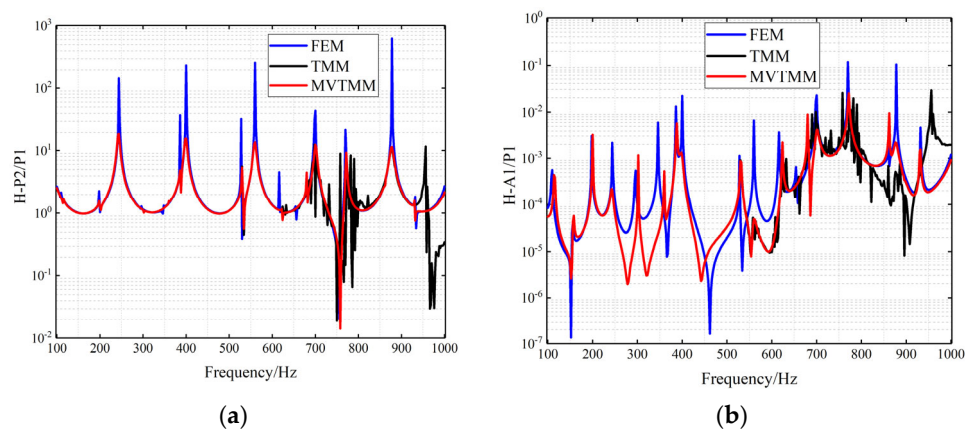


Figure 11. The comparison of theory and simulation. (a) Comparison of H-P2/P1, (b) Comparison of H-A1/P1.

In order to further validate the accuracy of the proposed method for predicting the FSI frequency domain vibration characteristics of the pipeline, we compared the calculated results with the experimental results, as illustrated in Figure 12. The comparison of modal data across various orders is presented in Table 6. As shown in Figure 12a, the trend of fluid vibration characteristics predicted by our method aligns closely with the experimental

results, with a maximum error of only 3.83% between the theoretical and experimental outcomes. In addition, it can be seen from Figure 12a that there is an anti-resonance peak at 760 Hz, which is caused by the FSI, but the anti-resonance peak obtained by the experiment is significantly higher than that obtained by the theoretical calculation. The reason for the difference may be that the pipe boundary condition adopted by the theoretical method is the ideal anchored boundary, which cannot be achieved completely in practice. Similarly, Figure 12b indicates that the pipeline flow-induced vibration characteristics predicted by our method are largely consistent with those observed in the experiment, exhibiting a maximum error of 4.35%. Notably, a formant at 460 Hz is detected in the experimental results for H-A1/P1, which is not anticipated by our theoretical model. It is speculated that this discrepancy may arise from boundary conditions within the actual pipeline failing to achieve absolute fixed support and rigid boundaries.

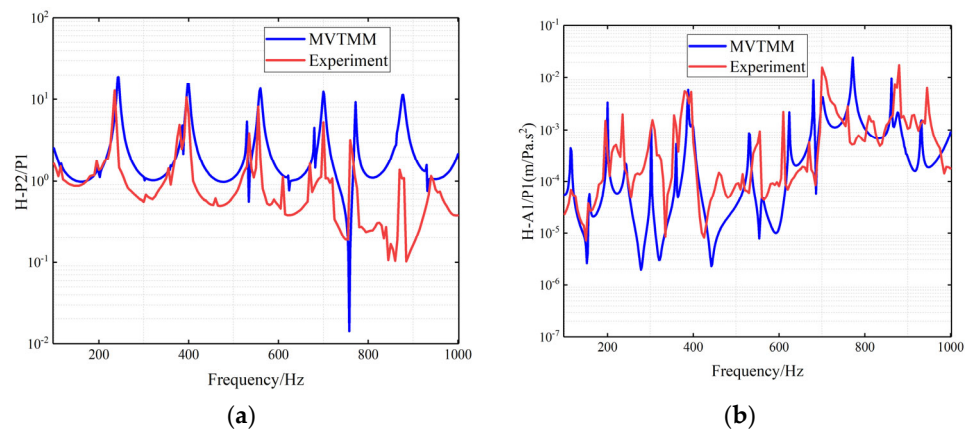


Figure 12. A comparison of the theory and the simulation. (a) Comparison of H-P2/P1, (b) Comparison of H-A1/P1.

Table 6. A comparison of the theory and the experiment.

The Experimental Result (Hz)	MVTMM		FEM	
	Natural Frequency (Hz)	Relative Error to Experiment (%)	Natural Frequency (Hz)	Relative Error to Experiment (%)
115	116	0.87	110	4.35
155	158	1.94	156	0.65
195	200	2.56	198	1.54
235	244	3.83	244	3.83
305	302	0.98	296	2.95
355	360	1.41	346	2.54
380	386	1.58	386	1.58
395	398	0.76	400	1.27
535	530	0.93	528	1.31
555	560	0.90	560	0.90
610	622	1.97	616	0.98
670	680	1.49	654	2.39
700	700	0.00	700	0.00
760	772	1.58	770	1.32
870	862	0.92	860	1.15
880	876	0.45	878	0.23
940	932	0.85	932	0.85

To illustrate the necessity of considering FSI in the analysis of hydraulic pipeline vibration characteristics, the H-P2/P1 index was utilized as a case to compare the outcomes of the classical water hammer model with those of the FSI model. The results are presented in Figure 13. It is evident that the classical water hammer model fails to account for

Poisson coupling and junction coupling; consequently, its predictions encompass only fluid vibration modes characterized by specific periodic patterns, neglecting pipeline vibration modes induced by FSI effects. Furthermore, the Poisson effect leads to a shift in fluid vibration modes towards lower frequencies.

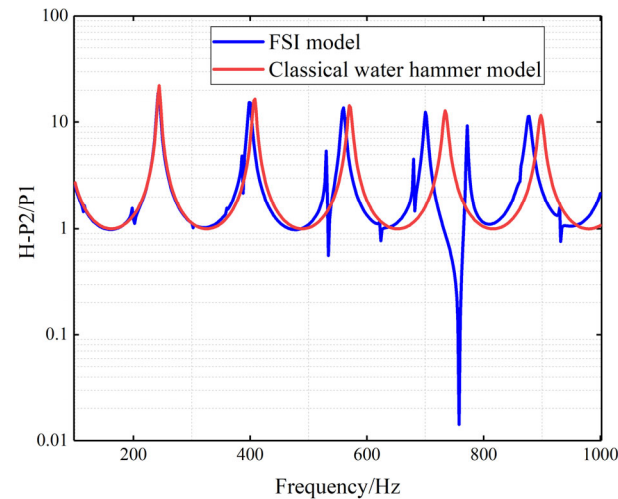


Figure 13. A comparison of the FSI model and the classical water hammer model.

5. Conclusions

In order to address the issue of high-frequency instability encountered when employing the TMM for long-span hydraulic pipeline systems, this paper first analyzes the instability mechanism from a mathematical perspective. Subsequently, a mixed variable approach is introduced to enhance the expression form of the transfer matrix, leading to the construction of a mixed variable transfer matrix specifically for pipeline units. By integrating this with the matrix representation of boundary conditions and utilizing a recursive algorithm for the mixed variable transfer matrix, an optimization technique known as the MVTMM is proposed. The stability and accuracy of this method are validated using data from Dube pipeline systems alongside the measured vibration data from a real hydraulic pipeline system. The main conclusions drawn from this study are as follows:

- (1) The MVTMM effectively mitigates high-frequency instability associated with the TMM, maintaining a global coefficient matrix dimension consistently at 28×28 . This ensures sustained efficiency, even when handling long-span hydraulic pipelines.
- (2) The MVTMM can accurately predict frequency domain vibration characteristics of hydraulic pipelines, demonstrating maximum errors of 3.03% when compared to Dube pipeline data and 4.35% relative to experimental data based on fluid excitation within real hydraulic pipeline systems.
- (3) Data obtained from the fluid excitation-based pipeline experiment indicate that FSI significantly influences frequency domain vibration characteristics in pipelines; thus, it should not be overlooked during predictive analyses.

The theoretical framework presented herein shows promise for engineering applications following validation and can be utilized for precise predictions regarding frequency domain vibration characteristics in ship-based long-span hydraulic pipeline systems. Future work will aim to extend this methodology into ship pipeline scenarios while considering complex constraints.

Author Contributions: Conceptualization, F.Z. and J.L.; methodology, F.Z. and J.L.; writing—original draft, F.Z.; writing—review and editing, Z.C.; visualization, X.T. supervision, L.H. and J.L. All authors have read and agreed to the published version of the manuscript.

Funding: This work was supported by the fund general projects of the National Key Laboratory on Ship Vibration and Noise (Grant No. JCKY2023207CI03).

Institutional Review Board Statement: Not applicable.

Informed Consent Statement: Not applicable.

Data Availability Statement: The original contributions presented in the study are included in the article; further inquiries can be directed to the corresponding author.

Conflicts of Interest: The authors declare no conflicts of interest.

Nomenclature

Uppercase letters

A	cross-sectional area
A^*	mechanical wave amplitude
E	Young's modulus
F	pipe shear force
G	shear modulus
I	moment of inertia
J	polar moment of inertia
K	fluid bulk modulus
L	length of pipe
M	pipe moment
P	fluid pressure
U	pipe velocity
ψ	pipe angular velocity
V	fluid velocity
Y	angular velocity impedance coefficient
Z	velocity impedance coefficient

Subscripts

e	end
f	fluid
i	inner
p	pipe
s	top
x, y	lateral coordinates
z	axial coordinate

Superscripts

D	reverse direction
H	transposed
U	forward direction
V	state variable
V_c	conjugate state variable

Lowercase letters

c	damping
e	thickness of pipe wall
f	pipe shear force
f^*	fluid friction force
k	stiffness
l	pipe node
m	pipe moment
p	fluid pressure
r	radius of cross section
u	pipe velocity
v	fluid velocity
v_f	fluid kinematic viscosity
μ	Poisson's ratio
ρ	density
τ	fluid shear force
φ	pipe angular velocity

λ	eigenvalue
<i>Matrices and vectors</i>	
$\mathbf{A}, \mathbf{B}, \mathbf{C}$	coefficient matrix of FSI model
\mathbf{D}	boundary matrix
\mathbf{I}	identity matrix
\mathbf{Q}	excitation vector
\mathbf{S}	eigenvector matrix
\mathbf{T}	transfer matrix
\mathbf{T}^*	FSI parameter matrix
$\mathbf{X}, \mathbf{Y}, \mathbf{Z}, \mathbf{W}$	mixed variable transfer matrix
$\boldsymbol{\phi}$	state vector of 14 variables in time domain
$\boldsymbol{\Phi}$	state vector of 14 variables in frequency domain

Appendix A. The Class TMM

The fundamental principle of class TMM is exemplified through the application of the L-MOC.

When the effect of the friction term is disregarded, Equations (1)–(14) can be uniformly expressed in the following matrix form:

$$\mathbf{A} \frac{\partial}{\partial t} \boldsymbol{\phi}(l, t) + \mathbf{B} \frac{\partial}{\partial z} \boldsymbol{\phi}(l, t) + \mathbf{C} \boldsymbol{\phi}(l, t) = 0 \tag{A1}$$

where \mathbf{A} , \mathbf{B} , and \mathbf{C} represent the coefficient matrices, while $\boldsymbol{\phi}(l, t)$ denotes the state variable vector comprising 14 variables:

$$\boldsymbol{\phi}(l, t) = (v, p, u_z, f_z, u_y, f_y, \varphi_x, m_x, u_x, f_x, \varphi_y, m_y, \varphi_z, m_z)$$

Let $\boldsymbol{\phi}(l, 0) = 0$. We applied the transformation of Equation (A1) to obtain the following:

$$s\mathbf{A}^* \boldsymbol{\Phi}(l, s) + \mathbf{B} \frac{\partial}{\partial z} \boldsymbol{\Phi}(l, s) = 0 \tag{A2}$$

where $\mathbf{A}^* = \mathbf{A} + \mathbf{C}/s$, and $\boldsymbol{\Phi}(l, s) = (V, P, U_z, F_z, U_y, F_y, \psi_x, M_x, U_x, F_x, \psi_y, M_y, \psi_z, M_z)$ represents the state variable in the frequency domain.

From Equations (1) and (3), it is evident that the impact of friction coupling manifests in the fluid shear force. Zielke [33] proposed a universal model for shear force in the frequency domain:

$$\tilde{\tau}(s) = \frac{\rho_f r_i}{\vartheta_1(jr_i \sqrt{s/\nu_f}) - 2} s(V - U_z) \tag{A3}$$

Therefore, the friction coupling is manifested in the correction of matrix \mathbf{A} within the frequency domain. This adjustment can be achieved by substituting the variable coefficients from Equation (A3) into their corresponding terms in the matrix.

To decouple Equation (A2), make the following transformations:

$$\boldsymbol{\Phi}(l, s) = \mathbf{S}(s)\boldsymbol{\eta}(l, s) \tag{A4}$$

Substituting Equation (A4) into Equation (A2) and subsequently eliminating variable \mathbf{A} yields the following result:

$$s\boldsymbol{\eta}(l, s) + \boldsymbol{\Lambda}(s) \frac{\partial \boldsymbol{\eta}(l, s)}{\partial z} = 0 \tag{A5}$$

where $\boldsymbol{\Lambda}(s) = \mathbf{S}(s)^{-1} \mathbf{A}^{*-1}(s) \mathbf{B} \mathbf{S}(s)$ represents the eigenvalue matrix of $\mathbf{A}^{*-1}(s) \mathbf{B}$, $\boldsymbol{\Lambda}(s)$ is the diagonal matrix, and $\mathbf{S}(s)$ corresponds to the associated eigenvector.

The general solution of Equation (A5) is

$$\boldsymbol{\eta}(l, s) = \mathbf{E}(l, s)\boldsymbol{\eta}_0(s) \tag{A6}$$

$\boldsymbol{\eta}_0(s)$ represents the constant term that is independent of position. $\mathbf{E}(l, s) = \text{diag}(\exp(-sl/\lambda_1), \exp(-sl/\lambda_2), \dots \text{etc})$, while λ denotes the eigenvalue associated with $\mathbf{A}^{*-1}(s)\mathbf{B}$.

Substituting Equation (A6) into Equation (A5) and integrating the boundary conditions at both ends of the pipeline yields the following:

$$\boldsymbol{\Phi}(l, s) = \mathbf{T}(l, s)\boldsymbol{\Phi}(l_0, s) \tag{A7}$$

where $\mathbf{T}(l, s) = \mathbf{S}(s)\mathbf{E}(l, s)\mathbf{S}(s)^{-1}$ denotes the field transfer matrix of the pipeline section, and l_0 indicates the initial position of the pipeline.

At both extremities of the pipeline, the boundary conditions are defined as follows:

$$\mathbf{D}_s(s)\boldsymbol{\Phi}(l_0, s) = \mathbf{Q}_s(s) \tag{A8}$$

$$\mathbf{D}_e(s)\boldsymbol{\Phi}(l, s) = \mathbf{Q}_e(s) \tag{A9}$$

where \mathbf{D}_s and \mathbf{D}_e represent the boundary matrices at each end of the pipeline, while \mathbf{Q}_s and \mathbf{Q}_e denote the excitation vectors corresponding to both ends of the pipeline.

Equations (A7)–(A9) are combined to obtain the following:

$$\boldsymbol{\Phi}(0, s) = \begin{bmatrix} \mathbf{D}_s(s) \\ \mathbf{D}_e(s)\mathbf{T}(l, s) \end{bmatrix}^{-1} \begin{bmatrix} \mathbf{Q}_s(s) \\ \mathbf{Q}_e(s) \end{bmatrix} \tag{A10}$$

By integrating Equations (A10) and (A7), the response of the state variable at any given position within the pipeline can be determined.

Appendix B. The Introduction of the PTMM

To illustrate the distinction between the TMM and the PTMM, consider the series pipeline system depicted in Figure A1. The total length of this pipeline system is represented as L , which is constructed by connecting N sub-pipe ends, each with a length of L_i .

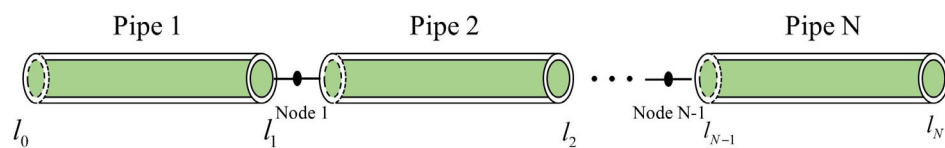


Figure A1. A schematic diagram of the series pipeline system.

For the classical TMM, the global transfer matrix of a piping system is obtained by the series multiplication of the transfer matrices of its individual pipeline segments, as follows:

$$\boldsymbol{\Phi}(l_N, s) = \mathbf{T}_{global}(s)\boldsymbol{\Phi}(l_0, s) \tag{A11}$$

$$\mathbf{T}_{global}(s) = \mathbf{T}(L_N, s) \dots \mathbf{T}(L_2, s)\mathbf{T}(L_1, s) \tag{A12}$$

When the total length of the pipeline is considerable, \mathbf{T}_{global} may become singular at high frequencies, resulting in instability phenomena.

The PTMM substitutes the global transfer matrix with a node-coupled matrix, thereby mitigating the numerical instability of matrix elements, as illustrated in Equation (A13):

$$\begin{bmatrix} \mathbf{D}_s(s) & 0 & 0 & 0 & 0 & 0 \\ \mathbf{T}(L_1, s) & -\mathbf{I} & 0 & 0 & 0 & 0 \\ 0 & \mathbf{T}(L_2, s) & -\mathbf{I} & 0 & 0 & 0 \\ 0 & 0 & 0 & \ddots & \ddots & 0 \\ 0 & 0 & 0 & 0 & \mathbf{T}(L_N, s) & -\mathbf{I} \\ 0 & 0 & 0 & 0 & 0 & \mathbf{D}_e(s) \end{bmatrix} \begin{bmatrix} \Phi(l_0, s) \\ \Phi(l_1, s) \\ \Phi(l_2, s) \\ \vdots \\ \Phi(l_{N-1}, s) \\ \Phi(l_N, s) \end{bmatrix} = \begin{bmatrix} \mathbf{Q}_s(s) \\ 0 \\ 0 \\ \vdots \\ 0 \\ \mathbf{Q}_e(s) \end{bmatrix} \quad (\text{A13})$$

References

- Païdoussis, M.P. Pipes conveying fluid: A fertile dynamics problem. *J. Fluids Struct.* **2022**, *114*, 103664. [\[CrossRef\]](#)
- Gao, P.; Yu, T.; Zhang, Y.; Wang, J.; Zhai, J. Vibration analysis and control technologies of hydraulic pipeline system in aircraft: A review. *Chin. J. Aeronaut.* **2021**, *34*, 83–114. [\[CrossRef\]](#)
- Qiu, Y.; Li, B.; Fu, X.; Yang, G.; Hu, J. Suppressing water hammer of ship steering systems with hydraulic accumulator. *Proc. Inst. Mech. Eng. Part E J. Process Mech. Eng.* **2014**, *228*, 136–148. [\[CrossRef\]](#)
- Wu, J.-H.; Liu, R.-J.; Duan, Y.; Sun, Y.-D. Free and forced vibration of fluid-filled laminated cylindrical shell under hydrostatic pressure. *Int. J. Press. Vessel. Pip.* **2023**, *202*, 104925. [\[CrossRef\]](#)
- Brown, F.T.; Tentarelli, S.C. Dynamic behavior of complex fluid-filled tubing systems—Part 1: Tubing analysis. *J. Dyn. Sys. Meas. Control* **2001**, *123*, 71–77. [\[CrossRef\]](#)
- Tentarelli, S.C.; Brown, F.T. Dynamic behavior of complex fluid-filled tubing systems—Part 2: System analysis. *J. Dyn. Sys. Meas. Control* **2001**, *123*, 78–84. [\[CrossRef\]](#)
- Wiggert, D.C.; Tijsseling, A.S. Fluid transients and fluid-structure interaction in flexible liquid-filled piping. *Appl. Mech. Rev.* **2001**, *54*, 455–481. [\[CrossRef\]](#)
- Deng, Y.; Jiao, Z.; Xu, Y. Frequency-domain analysis of fluid-structure interaction in aircraft hydraulic pipeline systems: Numerical and experimental studies. *J. Zhejiang Univ.-Sci. A* **2024**, *25*, 605–617. [\[CrossRef\]](#)
- Davidson, L.; Samsury, D. Liquid-structure coupling in curved pipes-II. *Shock. Vib. Bull.* **1972**, *43*, 123–135.
- Tentarelli, S.C. *Propagation of Noise and Vibration in Complex Hydraulic Tubing Systems*; Lehigh University: Bethlehem, PA, USA, 1990.
- Tijsseling, A.S.; Lambert, M.F.; Simpson, A.R.; Stephens, M.L.; Vítkovský, J.P.; Bergant, A. Skalak's extended theory of water hammer. *J. Sound Vib.* **2008**, *310*, 718–728. [\[CrossRef\]](#)
- Xu, Y.; Jiao, Z. Exact solution of axial liquid-pipe vibration with time-line interpolation. *J. Fluids Struct.* **2017**, *70*, 500–518. [\[CrossRef\]](#)
- Li, T.; Rui, X.; Zhang, J.; Zhang, L. Riccati transfer equations for fluid structure interaction in liquid-filled piping systems. *Heliyon* **2023**, *9*, e15923.
- Łuczko, J.; Czerwiński, A. Three-dimensional dynamics of curved pipes conveying fluid. *J. Fluids Struct.* **2019**, *91*, 102704. [\[CrossRef\]](#)
- Sreejith, B.; Jayaraj, K.; Ganesan, N.; Padmanabhan, C.; Chellapandi, P.; Selvaraj, P. Finite element analysis of fluid-structure interaction in pipeline systems. *Nucl. Eng. Des.* **2004**, *227*, 313–322. [\[CrossRef\]](#)
- Keramat, A.; Tijsseling, A.; Hou, Q.; Ahmadi, A. Fluid-structure interaction with pipe-wall viscoelasticity during water hammer. *J. Fluids Struct.* **2012**, *28*, 434–455. [\[CrossRef\]](#)
- Ahmadi, A.; Keramat, A. Investigation of fluid-structure interaction with various types of junction coupling. *J. Fluids Struct.* **2010**, *26*, 1123–1141. [\[CrossRef\]](#)
- Liu, G.; Li, Y. Vibration analysis of liquid-filled pipelines with elastic constraints. *J. Sound Vib.* **2011**, *330*, 3166–3181. [\[CrossRef\]](#)
- Zhang, L.; Tijsseling, S.; Vardy, E. FSI analysis of liquid-filled pipes. *J. Sound Vib.* **1999**, *224*, 69–99. [\[CrossRef\]](#)
- Xu, Y.; Johnston, D.N.; Jiao, Z.; Plummer, A.R. Frequency modelling and solution of fluid-structure interaction in complex pipelines. *J. Sound Vib.* **2014**, *333*, 2800–2822. [\[CrossRef\]](#)
- de Jong, C.A. Analysis of pulsations and vibrations in fluid-filled pipe systems. In Proceedings of the International Design Engineering Technical Conferences and Computers and Information in Engineering Conference, Boston, MA, USA, 17–20 September 1995; pp. 829–834.
- Li, S. *Dynamic Analysis of Fluid-Structure Interaction of Pipe Systems Conveying Fluid*; Harbin Engineering University: Harbin, China, 2015.
- Tanaka, K.; Kikuchi, K.; Okumura, A. Improvement of computation accuracy in transfer matrix method vibration analysis by using a branching process. *J. Sound Vib.* **1981**, *76*, 587–590. [\[CrossRef\]](#)
- Wang, Z. *The Vibration Properties Analyzation and Damage Detection for the Complex Multi-Span Pipe Conveying Fluid*; Wuhan University of Technology: Wuhan, China, 2019.
- Li, T.; Rui, X.; Zhang, J.; Yue, Q.; Miao, Y. Stability and orthogonality of fluid-structure interaction transfer matrix for liquid-filled pipeline systems. *J. Fluids Struct.* **2024**, *126*, 104088. [\[CrossRef\]](#)

26. Uhrig, R. The transfer matrix method seen as one method of structural analysis among others. *J. Sound Vib.* **1966**, *4*, 136–148. [[CrossRef](#)]
27. Li, Y. *Study on Vibration and Noise and Its Characteristics of Pipeline Systems Considering Fluid-Structure Interaction*; Harbin Engineering University: Harbin, China, 2011.
28. Zhang, Y.; Gao, Q. Stability analysis of the mixed variable method and its application in wave reflection and transmission in multilayered anisotropic structures. *Arch. Appl. Mech.* **2020**, *90*, 127–146. [[CrossRef](#)]
29. Cao, Y.; Liu, G.; Hu, Z. Stability improvement of the transfer matrix method when calculating the high frequency vibration of a pipeline conveying fluid. *J. Vib. Shock.* **2024**, *43*, 138–145.
30. Quan, L.; Sun, B.; Zhao, J.; Li, D. Frequency response analysis of fluid-structure interaction vibration in aircraft bending hydraulic pipe. *Xibei Gongye Daxue Xuebao/J. Northwestern Polytech. Univ.* **2018**, *36*, 487–495. [[CrossRef](#)]
31. Guo, X.; Ge, H.; Xiao, C.; Ma, H.; Sun, W.; Li, H. Vibration transmission characteristics analysis of the parallel fluid-conveying pipes system: Numerical and experimental studies. *Mech. Syst. Signal Process.* **2022**, *177*, 109180. [[CrossRef](#)]
32. Tijsseling, A.S.; Vardy, A.E. 20 years of FSI experiments in Dundee. *Ajp Heart Circ. Physiol.* **2005**, *296*, H1089–H1095.
33. Zielke, W. Frequency-Dependent Friction in Transient Pipe Flow. *J. Basic Eng.* **1968**, *90*, 109–115. [[CrossRef](#)]

Disclaimer/Publisher’s Note: The statements, opinions and data contained in all publications are solely those of the individual author(s) and contributor(s) and not of MDPI and/or the editor(s). MDPI and/or the editor(s) disclaim responsibility for any injury to people or property resulting from any ideas, methods, instructions or products referred to in the content.